Check for updates

Chemistry–A European Journal
Research Article
doi.org/10.1002/chem.202400690
Chemistry Europe
European Chemical Societies Publishing
www.chemeurj.org

Enabling High Activation of Glucose-6-Phosphate Dehydrogenase Activity Through Liquid Condensate Formation and Compression

Michel W. Jaworek,*[a] Rosario Oliva,*[b] and Roland Winter*[a]

Droplet formation via liquid–liquid phase separation is thought to be involved in the regulation of various biological processes, including enzymatic reactions. We investigated a glycolytic enzymatic reaction, the conversion of glucose-6-phosphate to 6-phospho-D-glucono-1,5-lactone with concomitant reduction of $NADP^+$ to NADPH both in the absence and presence of dynamically controlled liquid droplet formation. Here, the nucleotide serves as substrate as well as the scaffold required for the formation of liquid droplets. To further expand the process parameter space, temperature and pressure dependent measurements were performed. Incorporation of the reactants in the liquid droplet phase led to a boost in enzymatic activity, which was most pronounced at medium-high pressures. The crowded environment of the droplet phase induced a marked increase of the affinity of the enzyme and substrate. An increase in turnover number in the droplet phase at high pressure contributed to a further strong increase in catalytic efficiency. Enzyme systems that are dynamically coupled to liquid condensate formation may be the key to deciphering many biochemical reactions. Expanding the process parameter space by adjusting temperature and pressure conditions can be a means to further increase the efficiency of industrial enzyme utilization and help uncover regulatory mechanisms adopted by extremophiles.

Introduction

The most common enzyme deficiency worldwide is glucose-6-phosphate dehydrogenase (G6PDH)[1] and at least 160 disease-causing mutations of G6DPH have been reported,[2,3] most of them being point mutations leading to single amino acid substitutions that produce G6PDH variants. It is therefore hardly surprising that this enzyme is the subject of intensive research. The homodimer catalyses the oxidation of glucose-6-phosphate (G6P) to 6-phospho-D-glucono-1,5-lactone (6PGL) with concomitant reduction of the nicotinamide adenine dinucleotide phosphate $NADP^+$ to NADPH in the first step of the pentose phosphate pathway, whose products in the further course of the reaction pathway are necessary for nucleotide biosynthesis and the glycolytic pathway.[4,5] NADPH serves as a proton and electron donor for a variety of reduction reactions and has the ability to protect the cell against oxidative damage by transferring its reducing power to glutathione disulphide.[6,7]

The effect of pressure on biomolecular systems has become a fascinating topic in recent years, not only due to the fact that a major part of microbial organisms on Earth thrive in the deep sea where pressures up to 1000 bar are encountered,[8–11] but also due to the use of pressure in the modulation of biomolecular processes. Previous studies have provided revealing insights into the behavior of enzymes at high hydrostatic pressure (HHP).[12–18] High pressures can stabilize proteins at high temperatures, can lead to an increase in the conformational flexibility and alter the substrate specificity or stereoselectivity of an enzyme.[9,18] In addition, a smaller volume of the transition state of the enzyme-substrate complex ($ES^{\#}$) compared to the partial molar volumes of the reactants upon compression, i.e., a negative activation volume $\Delta V^{\#}$, results in an increased reaction rate. Different from temperature variation to modulate enzyme activity, pressure is still a largely unexplored parameter for improving the stability and activity of enzymes which are very sensitive to volume (packing) and hydration changes.[12,18–20]

In recent years, biochemical processes have been increasingly scrutinised at cellular crowding conditions as the cell interior is densely packed with various biomacromolecules (~200–400 g/L) which occupy about 40% of the volume.[21] Cellular crowding affects fundamental processes including DNA replication,[22] diffusion,[23,24] protein folding,[25–27] thermal stability,[28,29] and enzymatic activity.[30–36] Predicting the effects of crowding on the kinetics of biomolecular reactions is anything but easily predictable as examples have been reported where the reaction rate was increased,[35,36] remained unchanged,[37] or the activity was significantly reduced.[34,38] The

[a] Dr. M. W. Jaworek, Prof. Dr. R. Winter
Physical Chemistry I - Biophysical Chemistry, Department of Chemistry and Chemical Biology, TU Dortmund University, Otto-Hahn-Strasse 4a, 44227 Dortmund, Germany
E-mail: michel.jaworek@tu-dortmund.de
roland.winter@tu-dortmund.de

[b] Dr. R. Oliva
Department of Chemical Sciences, University of Naples Federico II, Via Cintia 4, 80126 Napoli, Italy
E-mail: rosario.oliva2@unina.it

Supporting information for this article is available on the WWW under https://doi.org/10.1002/chem.202400690

© 2024 The Authors. Chemistry - A European Journal published by Wiley-VCH GmbH. This is an open access article under the terms of the Creative Commons Attribution License, which permits use, distribution and reproduction in any medium, provided the original work is properly cited.

© 2024 The Authors. Chemistry - A European Journal published by Wiley-VCH GmbH

excluded volume effect, changes in the conformational dynamics of the enzyme, hydration changes, cosolute-induced changes of the activity coefficients and diffusion resistance of the reactants as well as product inhibition in the highly crowded environment can contribute to the overall reaction rate and enzymatic efficiency.[31,34,39–41]

Macromolecular crowding also has the ability to induce liquid-liquid phase separation (LLPS) formed by proteins and protein-nucleic acid mixtures at high concentrations. LLPS is a thermodynamic phenomenon in which molecules assemble to form a dense liquid phase, often a condensed droplet phase, which is separated from the diluted bulk phase. Such liquid condensates serve as multifunctional membraneless organelles in cells, allowing, for example, compartmentalization of reactions, buffering of molecules or midcell localization during cell division. In some other cases, they can also lead to pathological diseases such as Parkinson's, and Alzheimer's after structural transformations of amyloidogenic proteins resulting in fibril formation.[42–46] The driving force of LLPS formation is generally based on weak multivalent interactions, such as electrostatic, H-bonding, hydrophobic, π–π, and cation–π interactions,[46,47] which are strongly affected by external conditions including pH, ionic strength, temperature, pressure and the types and concentrations of excipients.[48] How exactly such LLPS systems influence enzymatic reactions, whether the reactants are preferentially located in the droplet phase and therefore concentrated or adopt a different active conformation, i.e. adopt a different conformational substate (CS) and different conformational dynamics, are still largely unexplored questions.[49–52] The incorporation of enzymes into liquid droplets can promote or inhibit their activity, and the progress of enzymatic reactions can also control the formation or dissolution of liquid droplets.

There is still insufficient knowledge regarding the dynamic relationship between the change in enzymatic activity due to incorporation into liquid droplets and the change in droplet state due to enzymatic conversion of droplet components. These relationships are very important as it is assumed that the droplet formation and dissolution is involved in many sequential enzymatic reactions in the compartmentalized biological cell. This study focuses on the enzymatic reaction of glucose-6-phosphate (G6P) and the cofactor $NADP^+$ by glucose-6-phosphate dehydrogenase (G6PDH), leading to 6-phospho-D-glucono-1,5-lactone (6PGL) with concomitant reduction of the cofactor $NADP^+$ to NADPH. The cofactor serves both as a substrate for the enzyme and as a scaffold for the formation of liquid condensates formed by the anionic nucleotide NADPH and the cationic poly-L-lysine (PLL). In a previous study, it was demonstrated that all reactants are located in the droplet phase.[53] We explored the combined effects of temperature, pressure and LLPS formation on the reaction as all these parameters can be expected to have some positive and additive effects, further enhancing the enzymatic activity.[12,13,54–56] To this end, the high-pressure stopped flow technology was used in combination with UV/Vis, fluorescence and Fourier-transform infrared (FTIR) spectroscopies as well as bright-field microscopy to follow the reaction kinetics with millisecond time resolution and to explore the stability and activity of the enzyme, which is dynamically coupled with droplet formation, over a wide temperature and pressure range.

Experimental Section

Sample Preparation

Lyophilized powder of glucose-6-phosphate dehydrogenase (G6PDH) from *Leuconostoc mesenteroides*, nicotinamide adenine dinucleotide $NADP^+$, glucose-6-phosphate (G6P) and poly-L-lysine (PLL, 15–30 kDa) were obtained from Sigma Aldrich and were used without further purification. HEPES buffer (100 mM 4-(2-hydroxyethyl)-1-piperazineethanesulfonic acid) with 1 mM $MgCl_2$ at pH = 7.4 was used to prepare the enzyme and substrate solutions.

High-Pressure Stopped-Flow (HPSF) Enzyme Kinetics

The enzyme reaction is based on a bi-bi mechanism consisting of four elementary steps, r_i, which are shown in Equation 1:[5]

$$\begin{aligned} r_1&: \; E + A + B \underset{k_{-1}}{\overset{k_1}{\rightleftarrows}} [E-A] + B \\ r_2&: \; [E-A] + B \underset{k_{-2}}{\overset{k_2}{\rightleftarrows}} [E-P_1-P_2] \\ r_3&: \; [E-P_1-P_2] \underset{k_{-3}}{\overset{k_3}{\rightleftarrows}} [E-P_2] + P_1 \\ r_4&: \; [E-P_2] + P_1 \underset{k_{-4}}{\overset{k_4}{\rightleftarrows}} E + P_2 + P_1 \end{aligned} \tag{1}$$

(E = G6PDH, A = $NADP^+$, B = G6P, P_1 = 6-phospho-D-glucono-1,5-lactone, P_2 = NADPH).

Some assumptions can be made allowing us to analyse the kinetic parameters in some detail. On the one hand, high concentrations of G6P were used to follow the time-dependent concentration change of NADPH, and on the other hand we utilize the fact that the equilibrium is on the side of the enzyme-$NADP^+$-complex due to its higher affinity compared to the G6P. Under these simplifications, the kinetics could be treated with the Michaelis-Menten equation for a pseudo-one substrate reaction (Eq. 2):[4,5]

$$v = \frac{v_{max}\,[S]}{K_{M,i} + [S]} = \frac{k_{cat,i}\,[E]_{tot}\,[S]}{K_{M,i} + [S]} \tag{2}$$

with [E] the enzyme concentration, [S] the substrate concentration, $K_{M,NADP^+} = (k_{-1} + k_2)/k_1$, and $K_{M,G6P} = (k_{-2} + k_3)/k_2$).

Following Eyring's theory of reaction rates, the activation volume, $\Delta V^{\neq}$, which describes the difference between the volume of the transition state (TS = $ES^{\neq}$) and the ground state of the enzyme-substrate complex (ES), can be determined through the pressure effect on the change of the reaction rate (Eq. 3a). The binding volume, ΔV_b, signifies the difference in the ES-complex volume and the unbound reactant state (E + S), and is related to the shift in the Michaels constant with pressure (Eq. 3b):[5,6]

$$\text{a)}\left(\frac{\partial \ln k_{cat}}{\partial p}\right)_T = -\frac{\Delta V^{\neq}}{RT};\ \text{b)}\left(\frac{\partial \ln K_M^{-1}}{\partial p}\right)_T = -\frac{\Delta V_b}{RT} \tag{3}$$

Due to different compressibilities of the reactants, the ES complex and the transition state, $\Delta V^{\neq}$-values can be positive or negative,

© 2024 The Authors. Chemistry - A European Journal published by Wiley-VCH GmbH

15213765, 2024, 28, Downloaded from https://chemistry-europe.onlinelibrary.wiley.com/doi/10.1002/chem.202400690 by Technische Universitaet Dortmund, Wiley Online Library on [14/07/2026]. See the Terms and Conditions (https://onlinelibrary.wiley.com/terms-and-conditions) on Wiley Online Library for rules of use; OA articles are governed by the applicable Creative Commons License

and they can also be dependent on the pressure amplitude. In a two-substrate reaction with a ternary complex mechanism, the interpretation of $\Delta V^{\neq}$ is more complicated.[53]

The initial concentration of the enzyme for all measurements after mixing inside the sample cell was 10 nM. The kinetic parameters (Michaelis constant $K_{M,NADP+}$, and turnover number $k_{cat,NADP+}$) were determined through the initial velocity ($v_0 = d[P]/dt$) from the slope of the linear fit of the time-dependent absorbance data at 340 nm by varying the $NADP^+$ concentration from 2.5 to 100 μM at a constant G6P concentration of 300 μM. Similarly, $K_{M,G6P}$ and $k_{cat,G6P}$ were measured at the same enzyme concentration by varying the G6P concentration from 5 to 1000 μM at a $NADP^+$ concentration of 40 μM.[4]

Enzyme activities at different pressures were measured using a high-pressure stopped-flow (HPSF) instrument (TgK Scientific), which allows recording reactions up to 2 kbar (1 bar $\hat{=}$ 0.1 MPa). The construction and operating principle of the high-pressure stopped-flow instrument is described in detail elsewhere.[19,57] After the rapid mixing process has taken place (dead time ~10 ms), the absorbance at 340 nm by using the Lambert-Beer law with the molar extinction coefficient $\varepsilon_{340\ nm} = 6220\ cm^{-1}M^{-1}$ of the product NADPH was measured up to 30 s to obtain the initial velocity. Kinetic studies were performed at 20 and 37 °C in HEPES buffer and in addition in 200 μM PLL (monomer concentration) using an external water circuit. The pressure was monitored using a high-pressure control unit and increased stepwise in 500 bar-steps up to 2000 bar. Upon achieving the desired pressures, the samples were equilibrated for 5 min.

Fourier-Transform Infrared (FTIR) Spectroscopy

Pressure and temperature dependent FTIR scans were performed using a Nicolet Magna 550 (Thermo Fisher Scientific) spectrometer equipped with a liquid-nitrogen-cooled MCT detector. Each FTIR spectrum was obtained by recording 128 scans at a spectral resolution of 2 cm^{-1} in the wavenumber range between 4000 and 650 cm^{-1}. The pressure of up to 10 kbar was generated with an automatic pneumatic pressure regulator (Diacells iGM Controller, Almax easyLab), which exerts pressure on the diamond anvil cell equipped with type IIa diamonds (Diacells VivoDac, Almax easyLab). In short, the sample was subjected to the desired pressure. Once the final pressure was reached, the sample was equilibrated for 5 min before the FTIR spectra were collected. Pressure was determined with co-added crystalline $BaSO_4$ as an internal pressure calibrator (following the band at ~983.5 cm^{-1}) with an accuracy of around 15 MPa).[58] An external circulating water thermostat controlled the required temperature in the cell.

First, the enzyme G6PDH was dialyzed against D_2O using Amicon Ultra (2 mL) centrifugation units with 10 kDa cutoff and subsequently lyophilized. The sample concentration was 50 mg mL^{-1} in HEPES buffer (+1 mM $MgCl_2$ in D_2O). For the temperature dependent measurements, the sample was first heated to the desired temperature and then equilibrated for ~5 min before the spectra were recorded. All spectra were processed with Happ-Genzel apodization using the Omnic 7.2 spectral processing software. Afterwards, the GRAMS AI 8.0 software was used to further process and analyse the spectra. After buffer subtraction and smoothing, normalisation of the area of the amide I' band (1700–1600 cm^{-1}) was performed. Based on two mathematical operations (Fourier self-deconvolution (FSD) and 2nd derivative spectra), the number and positions of the subbands of the amide I' band region of G6PDH could be determined into six subbands. The relative changes in the population of secondary structure elements were obtained via mixed Gaussian–Lorentzian line shape functions in the linear combination fitting procedure.[59]

Microscopy

The microscopy experiments were carried out 30 min after preparation of the sample solution (1 mM $NADP^+$, 1 mM G6P, 5 mM PLL (expressed per lysine monomeric concentration), for the fluorescence measurements 1 mol% Alexa 488-labelled PLL was added, and 0.5 μM G6PDH). Fluorescent labeling of PLL was performed using the Alexa Fluor 488 protein labeling kit from Thermo Fisher scientific). Bright-field light microscopy images were recorded on an Eclipse TE2000-U microscope (Nikon Inc.) using a Nikon Plan Fluor 20x objective (NA 0.45, WD 7.4) and additionally a X–Lite™-120 fluorescence Illumination System EXFO and a F41-054 HQ-Set filter ($\lambda_{ex.} = 480$ nm, $\lambda_{em} = 527$ nm) for the fluorescence mode. For pressure application, a home-built pressure cell equipped with flat diamond windows of 0.8 mm thickness was used and pressure was applied hydrostatically with a high-pressure hand pump. Temperature was controlled by a circulating water bath. The processing of the microscopy snapshots was done with ImageJ.

For statistical analysis, the number of droplets was set to 50 and 4×250 μm^2 areas were examined to determine the droplet size, circularity, and number of droplets.

Turbidity Measurements

Light scattering measurements were carried out using a K2 fluorometer from ISS (Champaign, IL, USA). An excitation wavelength of 400 nm was used and the emission was collected at 403 nm. For the pressure-dependent measurements, an ISS high-pressure cell with 1 cm thick quartz windows was used. With the help of an external water bath, the temperature inside the pressure cell was adjusted during the measurements. A small quartz cuvette filled with the sample solution was sealed with DuraSeal laboratory stretch film and placed inside the high-pressure cell. The pressure was applied hydrostatically via a manual high-pressure hand pump. The pressurized medium was water. Here, the experiments were carried out starting 30 min after preparation of the sample solution (65 μM $NADP^+$, 1 mM G6P, 320 μM PLL (monomer concentration), 0.5 μM G6PDH).

Fluorescence Spectroscopy

Fluorescence emission spectra of the enzyme G6PDH in neat buffer conditions without $NADP^+$ or NADPH and upon addition of PLL (500 μM) were recorded by using a K2 spectrofluorometer from ISS (Champaign, IL, USA). Due to the strong fluorescence signal from $NADP^+$ and NADPH in the investigated wavelength range, it was not possible to record the fluorescence from the enzyme in the presence of $NADP^+$ or NADPH. Consequentially, the fluorescence spectra were recorded under non-phase separating conditions. The wavelength of excitation was set to 280 nm, the emission was collected in the range 310–450 nm. Both the excitation and emission monochromator slits were set to 8 nm. The spectra were recorded between 1 bar and 2000 bar. To this end, a high-pressure cell system from ISS was used. Briefly, the samples were loaded in a 300 μL quartz cuvette with a path length of ~0.3 cm. Then, the cuvette was sealed with a thin polyethylene membrane which allows the pressure to be transmitted to the sample. The sealed cuvette was placed in the high-pressure cell and filled with water. The high-pressure cell was then connected, through a capillary tube, to a manual water pump which allows pressure transmission.

© 2024 The Authors. Chemistry - A European Journal published by Wiley-VCH GmbH

15213765, 2024, 28, Downloaded from https://chemistry-europe.onlinelibrary.wiley.com/doi/10.1002/chem.202400690 by Technische Universitaet Dortmund, Wiley Online Library on [14/07/2026]. See the Terms and Conditions (https://onlinelibrary.wiley.com/terms-and-conditions) on Wiley Online Library for rules of use; OA articles are governed by the applicable Creative Commons License

The temperature of the cell system (20 °C) was controlled by means of a water bath directly connected to the cell. The center of mass (CM, in nm) was determined in order to precisely record the wavelength shift of the fluorescence spectrum.[60]

Results

Temperature and Pressure Dependent Stability of the Enzyme

To characterize the structural stability of G6PDH under the temperature and pressure conditions studied, we first determined the secondary structural changes of the protein using Fourier-transform infrared (FTIR) spectroscopy, covering a temperature range from 20 to 70 °C and a pressure range from 1 bar to 5.5 kbar. Figure 1 shows the normalised temperature-dependent and pressure-dependent FTIR spectra of the enzyme as well as the corresponding changes in secondary structural elements derived from the curve fitting analysis. At ambient pressure and 20 °C, the amide I' band of the protein shows a broad band at 1648 cm^{-1}, which can be deconvoluted into its secondary structure elements. G6PDH exhibits high contents of intramolecular β-sheets (~26 %) and α-helices (~32 %), in good agreement with crystallographic data.[61] The minor differences between the X-ray diffraction and FTIR data can result from different absorption coefficients of the various secondary structure elements. Upon temperature-induced unfolding, the α-helix content decreases and aggregation of the protein, detected at 1618 cm^{-1} and 1685 cm^{-1}, due to formation of intermolecular molecular β-sheets takes place, i.e., unfolding is followed by aggregation of the protein at high temperatures. The transition mid-point temperature, T_m, is located at 50.0 ± 1.1 °C, which is in the same range observed in other G6PDHs from other organisms.[62,63] Table SI 1 summarizes the value for thermal unfolding of each structural component, which are all located at around 50 °C, indicating high cooperativity of the process. The temperature-induced process of protein unfolding and subsequent aggregation was found to be irreversible. Upon an increase of pressure, a shift of the amide I' band of the enzyme towards lower wavenumbers was observed only, which is caused by a pressure-induced compression of the chemical bonds, equivalent to changes of the force constant of the C=O-stretching vibration. Minor conformational changes seem to take place beyond 2.5–3 kbar, only.

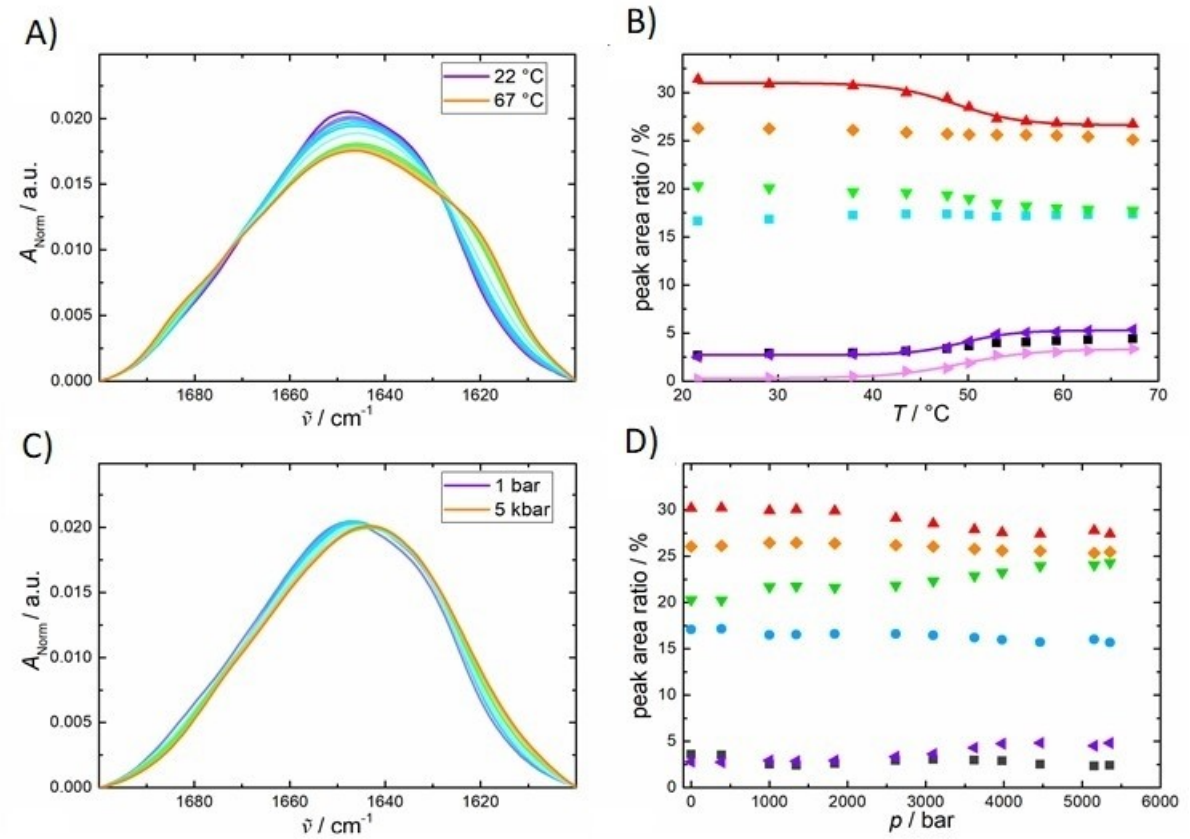

Figure 1. Temperature and pressure dependent FTIR absorption data of 5 wt % G6PDH in HEPES buffer (A–D). Left: normalized amide I' band, right: respective secondary structure elements of temperature and pressure induced changes: β-turns (1685 cm^{-1}, black), turns and loops (1671 cm^{-1}, blue), α-helices (1654 cm^{-1}, red), random coils (1642 cm^{-1}, green), intramolecular β-sheets (1630 cm^{-1}, orange), intermolecular β-sheets (1618 cm^{-1}, pink), and side chains (1608 cm^{-1}, purple). The temperature-dependent measurements were recorded at ambient pressure (1 bar), the pressure dependent measurements at $T = 20$ °C.

© 2024 The Authors. Chemistry - A European Journal published by Wiley-VCH GmbH

15213765, 2024, 28, Downloaded from https://chemistry-europe.onlinelibrary.wiley.com/doi/10.1002/chem.202400690 by Technische Universitaet Dortmund, Wiley Online Library on [14/07/2026]. See the Terms and Conditions (https://onlinelibrary.wiley.com/terms-and-conditions) on Wiley Online Library for rules of use; OA articles are governed by the applicable Creative Commons License

15213765, 2024, 28, Downloaded from https://chemistry-europe.onlinelibrary.wiley.com/doi/10.1002/chem.202400690 by Technische Universitaet Dortmund, Wiley Online Library on [14/07/2026]. See the Terms and Conditions (https://onlinelibrary.wiley.com/terms-and-conditions) on Wiley Online Library for rules of use; OA articles are governed by the applicable Creative Commons License

Temperature and Pressure Dependent Stability of the Droplet Phase

Subsequently, the stability of the droplet phase of PLL/NADPH was evaluated for the temperature and pressure range used for modulation of the enzymatic reaction. To determine the temperature and pressure dependent phase behavior of the PLL/NADPH system, bright-field light microscopy studies were carried out. Monitoring fluorescence-labeled PLL confirmed sequestration of the homopolymer in the droplet phase (Figure SI1). Figure 2 displays light microscopy snapshots of droplets after initiation of the phase separation (mixing 1 mM $NADP^+$, 1 mM G6P, 5 mM PLL (per monomer concentration) and 0.5 μM G6PDH) at selected temperatures and 1 bar as well as at selected pressures for $T = 20\,°C$. Micrometer-sized droplets less than 2.5 μm (Fig SI2), as also reported in Ref. [53], were clearly visible at all temperatures measured, which is characteristic for the liquid-liquid phase-separated state. Above about 60 °C, the number of droplets decreased. When cooled down from 80 to 20 °C, the number of droplets increased again to the original level, revealing reversibility of the process. As far as pressure stability is concerned, the number of droplets and the droplet size were found to remain essentially constant and droplets were still visible at 1.5 kbar, the highest pressure recorded here. Despite the small size and hence suboptimal image quality, most of the PLL/NADPH droplets appeared to have circular shapes. The statistics of droplet abundance per analyzed area unit, the diameter, and the circularity of the droplets determined from the snapshots as a function of temperature and pressure are shown in Figure SI2.

Complementary turbidity (light scattering) measurements were carried out at 403 nm using a UV/Vis spectrometer to confirm the observations obtained from the microscopy data (Figure SI3). The data showed that the cloud-point temperatures and pressures of the LLPS state were not reached in the temperature and pressure range covered in the enzyme kinetic measurements, i.e., up to 37 °C and 2 kbar, respectively.

Modulation of Enzyme Kinetics by Temperature, Pressure, and LLPS

The influence of pressure on the enzymatic reaction in connection with liquid-liquid phase separation has not yet been investigated. Figure SI4 displays the time course of the UV/Vis absorbance data at 340 nm, reflecting the formation of the product NADPH at 20 °C in neat buffer and in the presence of PLL at 37 °C. First, the kinetic parameters of the redox reaction at ambient pressure (1 bar) were compared with literature data and found to be in good agreement, the Michaelis constants being $K_{M,G6P} = 81\,\mu M$ and $K_{M,NADP+} = 5\,\mu M$, respectively.[5] The small differences observed can be attributed to the different buffer systems used. Subsequently, the enzymatic activity was investigated under pressure by using a high-pressure stopped-flow system. Figures 3 A, B show the Michaelis Menten plots for the redox reaction of $NADP^+$ (at constant concentration) and G6P (varied concentration) catalyzed by G6PDH at different temperatures (20 and 37 °C). The initial reaction rate, v_0, was found to increase markedly with increasing temperature for all substrate concentrations and pressures. On the other hand, a different kinetic behavior was induced with increasing pressure, since the reaction rate was found to decrease at ~500 bar and a marked activity beyond 1000 bar was not quantifiable anymore. These observations are clearly reflected in the Michaelis Menten kinetic data (Figure 4, orange bars for 20 °C, red bars for 37 °C). With both increasing temperature, T, and pressure, p, the Michaelis constant $K_{M,G6P}$ was found to increase (with p even 5–10 fold), i.e., the affinity of the substrate decreased with growing temperature and pressure. The decreased affinity at high temperature is probably due to the higher conformational

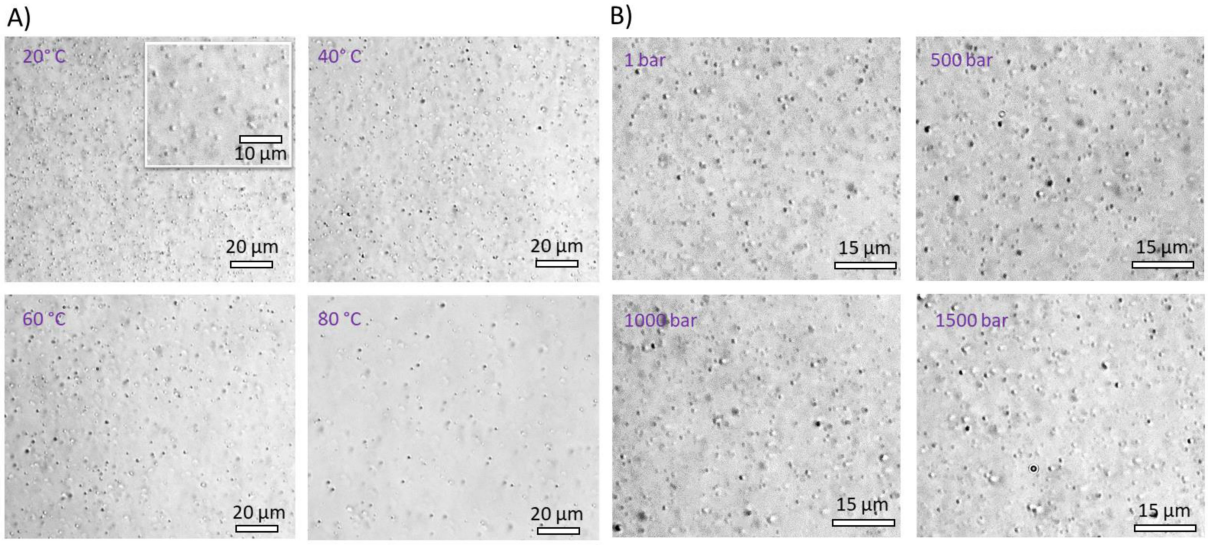

Figure 2. Representative broad-field light microscopy snapshots of the LLPS system PLL/NADPH (based on the composition of 1 mM $NADP^+$, 1 mM G6P, 5 mM PLL (per lysine monomer concentration) and 0.5 μM G6PDH after 30 min) as a function of A) temperature at 1 bar and B) pressure at $T = 20\,°C$. The inset displays an enlargement of the snapshot of the LLPS system at 20 °C.

© 2024 The Authors. Chemistry - A European Journal published by Wiley-VCH GmbH

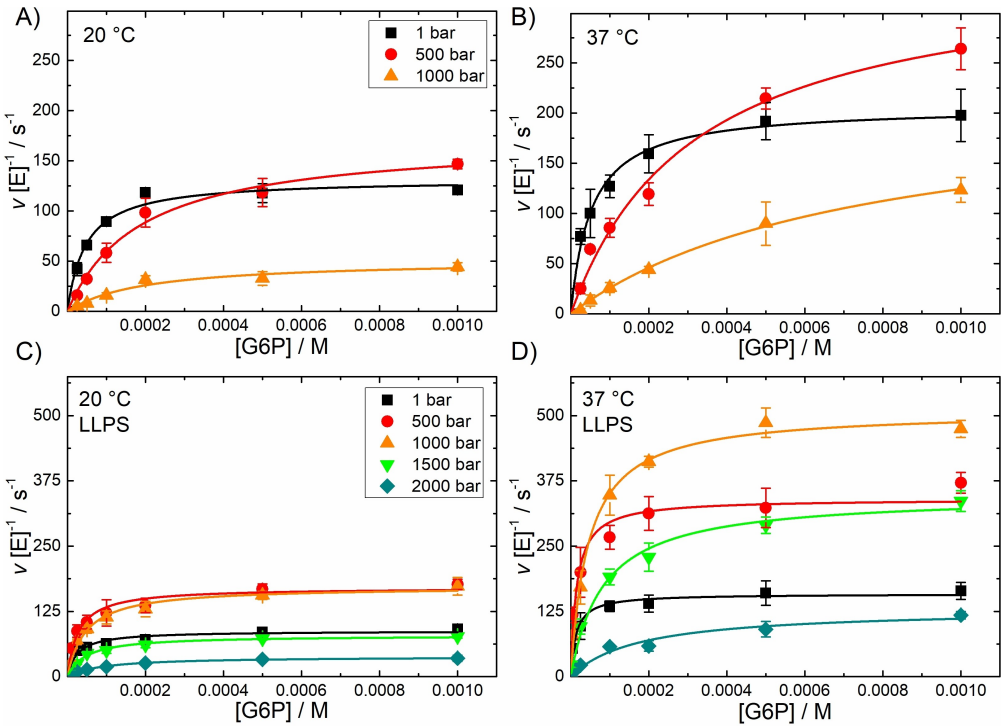

Figure 3. Michaelis–Menten plots for the redox reaction of $NADP^+$ catalyzed by 10 nM G6PDH at different substrate concentrations, [G6P], and pressures, *p*, at $T = 20\,°C$ (A, C) and $T = 37\,°C$ (B, D). For Figures 3A, B the initial reaction velocity was measured in neat HEPES buffer at a constant $NADP^+$ concentration of 40 μM, whereas for Figs. 3 C, D 200 μM PLL (monomer concentration) was added to the buffer to form the NADPH/PLL droplets (LLPS state) immediately after the formation of the product NADPH.

dynamics of the protein. With increasing temperature, the turnover number, $k_{cat,G6P}$, increased 1.5–3 fold, and upon compression the $k_{cat,G6P}$ value reached a maximum around 500 bar. Regarding the catalytic efficiency, $k_{eff,G6P} = k_{cat,G6P}/K_{M,G6P}$, both increasing temperature and pressure at neat buffer conditions did not lead to a marked increase of the catalytic efficiency owing to a compensating effect of $k_{cat,G6P}$ and $K_{M,G6P}$.

Next, we recorded the corresponding kinetic data in the presence of LLPS. To ensure spontaneous formation of NADPH/PLL droplets as the enzymatic reaction proceeds, a concentration of 200 μM PLL (per monomer concentration) was used. Figures 3 C, D reveal drastic differences in the kinetic traces obtained under these conditions at the two temperatures 20 and 37 °C. The activity of the enzyme could be recorded even up to a pressure of 2000 bar under these solution conditions, i.e., in the presence of LLPS induced by PLL and the product NADPH, drastically higher reaction rates were determined at all temperature and pressure conditions. Generally, whereas an increase of K_M can be accounted for by considering diffusion resistance in a crowded environment, a reduction of K_M, corresponding to an increase of affinity, can be attributed to changes in activity coefficients. The Michaelis constant was found to be lower, i.e., the affinity of the substrate was higher compared to the reaction in pure buffer solution. The $K_{M,G6P}$ values increased by a factor of two only upon compression at 20 °C, and the $k_{cat,G6P}$ values reached a high maximum in the droplet system at about 1000 bar for both temperatures, followed by a subsequent decrease at higher pressures. The optimum conditions for the catalytic efficiency, $k_{eff,G6P}$, were reached at 500 bar for $T = 37\,°C$, with $k_{eff,G6P}$ values being almost 10 times larger compared to the $k_{eff,G6P}$ value under ambient conditions (1 bar, 20 °C). These results clearly show that the formation of droplets drastically improves the enzymatic activity with regard to all kinetic parameters.

Additionally, we investigated the enzymatic reaction by varying the $NADP^+$ concentration at constant G6P concentration for $T = 20\,°C$ (Figs. SI5, SI6). The Michaelis constant $K_{M,NADP+}$ was found to be significantly lower compared to $K_{M,G6P}$ (by a factor of ~10), which indicates a much higher affinity of the substrate, in accordance with literature data.[53] While $K_{M,G6P}$ increased with increasing pressure, $K_{M,NADP+}$ did not change significantly upon compression within the experimental error bars. As expected, the trend for the turnover number for both substrates was found to be similar up to 1 kbar. As a result of the different Michaelis constants, a significantly higher catalytic efficiency was determined for the $NADP^+$-concentration dependent reaction, which decreased markedly upon compression to 1 kbar.

The activation volume $\Delta V^{\neq}$ of the enzymatic reaction could be determined from the pressure dependence of k_{cat} (Eq. 3a, the data are shown in Table 1). $\Delta V^{\neq}$ describes the difference between the volumes of the transition state ($ES^{\neq}$) and the enzyme-substrate complex (ES). Consequently, an increase in $k_{cat}(p)$ values upon compression implies that the volume of the transition state is more compact than the volume of the ES complex, which can be attributed to filling of void volume,

© 2024 The Authors. Chemistry - A European Journal published by Wiley-VCH GmbH

15213765, 2024, 28, Downloaded from https://chemistry-europe.onlinelibrary.wiley.com/doi/10.1002/chem.202400690 by Technische Universitaet Dortmund, Wiley Online Library on [14/07/2026]. See the Terms and Conditions (https://onlinelibrary.wiley.com/terms-and-conditions) on Wiley Online Library for rules of use; OA articles are governed by the applicable Creative Commons License

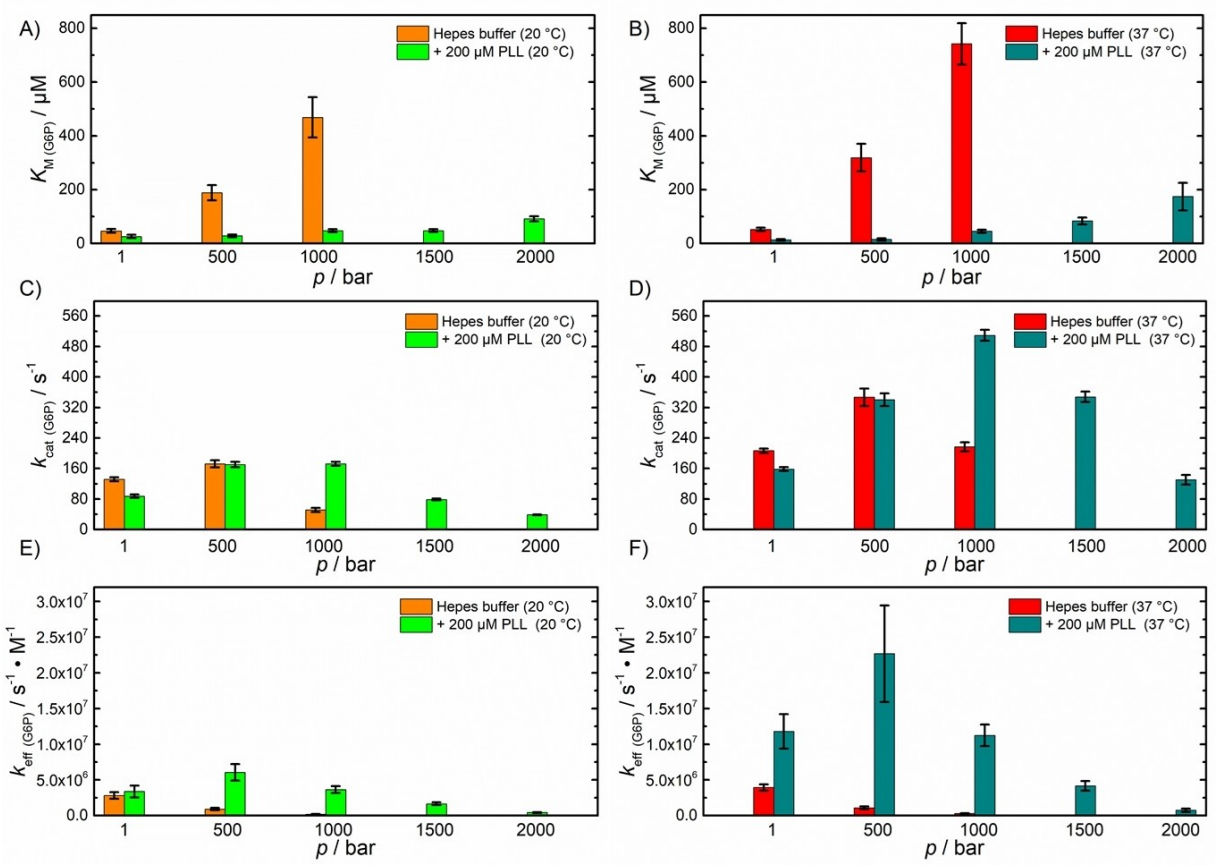

Figure 4. Pressure dependence of the kinetic constants for the redox reaction of $NADP^+$ and G6P catalyzed by G6PDH at different temperatures and different solution conditions, by varying the G6P concentration. A, B) Michaelis constant, K_M; C, D) turnover number, k_{cat}; E, F) catalytic efficiency, k_{eff}.

Table 1. Calculated apparent activation volumes, $\Delta V^{\neq}$, in the low pressure (k_{cat} ↑) and high pressure (k_{cat} ↓) regime, and the binding volumes, ΔV_b, for the redox reaction of G6P catalyzed by G6PDH at two different temperatures, 20 and 37 °C.

	$\Delta V^{\neq}$/mL mol^{-1}		ΔV_b/mL mol^{-1}
	k_{cat} ↑ (low p regime)	k_{cat} ↓ (high p regime)	K_M ↑
HEPES buffer (20 °C)	−13.1 ± 0.6	58.9 ± 2.3	56.2 ± 6.9
+ 200 µM PLL	−32.6 ± 1.3	36.5 ± 0.9	15.7 ± 2.9
HEPES buffer (37 °C)	−26.7 ± 1.8	24.2 ± 0.5	64.6 ± 13.6
+ 200 µM PLL	−30.1 ± 5.4	35.2 ± 9.0	31.4 ± 14.8

hydration changes or minor conformational changes within the active site of the enzyme during the course of the reaction. In the case of a two-substrate reaction, the initial rate-determining step might change beyond a certain pressure, e.g. from k_2 to k_3, or k_3 can no longer be neglected (Eq. 1). It is also possible that the activation volume is not pressure-independent, i.e., a compressibility term must be taken into account; at these rather low pressures such an effect is rather unlikely in this pressure range, however.[54] Surprisingly, at high pressures, the $\Delta V^{\neq}$ values determined were found to be positive (Table 1), leading to an apparent decrease of k_{cat} in the high-pressure regime, which can be explained by a change in the structure of the enzyme (see below). Of note, at low substrate concentrations, which is not the case here, the reaction rate is also dependent on the Michaelis constant, i.e., $\Delta V^{\neq}$ should also include the activation volume for substrate binding. The binding volume itself, ΔV_b, could be determined from $K_M(p)$ according to Eq. 3b. These data show that the reactants (E, S) have a smaller partial molar volume compared to the ES complex, i.e. $\Delta V_b > 0$, i.e., binding becomes less favourable upon compression, the effect being smaller in the droplet phase compared to neat buffer conditions.

In order to explain the changes in the observed activity of the enzyme beyond 500 bar in neat buffer, fluorescence emission spectra of the enzyme upon excitation at 280 nm were recorded in the pressure range from 1 to 2000 bar. The

© 2024 The Authors. Chemistry - A European Journal published by Wiley-VCH GmbH

15213765, 2024, 28, Downloaded from https://chemistry-europe.onlinelibrary.wiley.com/doi/10.1002/chem.202400690 by Technische Universitaet Dortmund, Wiley Online Library on [14/07/2026]. See the Terms and Conditions (https://onlinelibrary.wiley.com/terms-and-conditions) on Wiley Online Library for rules of use; OA articles are governed by the applicable Creative Commons License

position of the emission of Trp spectra is known to sensitively depend on the environment surrounding the residue.[64,65] In our case, the enzyme G6PDH is a dimer with several Trp residues located at the interface between the two monomer units and, consequentially, are hidden from the solvent. Thus, changes in the maximum of emission of Trp spectra are indicative of the dimerization state of the enzyme. Figure 5 depicts the wavelength at the maximum of emission of G6PDH in neat buffer and upon addition of PLL (500 μM) as function of pressure. In both cases, a red shift of the emission band could be observed with increasing pressure, which is due to the exposure of the Trp residues to the surrounding water molecules following dissociation of the G6PDH dimer into its monomeric units. A plateau value was reached around 700 bar, indicating that the dissociation was complete. The reported data are in excellent agreement with the observed pressure-dependent activity data of the enzyme, showing reduced activities beyond ~500 bar due to the pressure-induced disassembly of the dimeric enzyme. As the active site is located close to the edge of the dimer interface, dimer formation is essential for effective enzymatic activity.[61] According to the high-pressure FTIR data, dissociation of the protein is not accompanied by a significant change in secondary structure (Figure 1). Finally, it should be noted, as Figure 4C clearly shows, that in the presence of PLL, the catalytic efficiency at 500 and 1000 bar of the reaction is higher than that of the reaction carried out without PLL. Combining this information with the data reported in Figure 5, it can be concluded that the phase separation counteracts the deleterious effect of pressure in promoting the dimer disassembly. Consequentially, the reaction still proceeds at a reasonable rate even at high pressure.

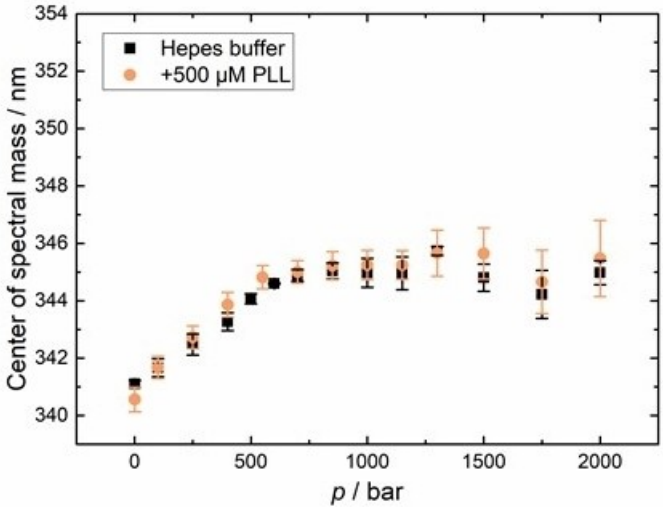

Figure 5. The center of spectral mass of tryptophan emission of G6PDH in HEPES buffer (black squares) and in the presence of 500 μM PLL (per monomer concentration, orange circles) as a function of pressure ($T = 20\,^{\circ}C$).

Discussion and Conclusions

High concentrations of proteins and nucleic acids can lead to an increased tendency for liquid-liquid phase separation of the solution.[42,43] Cellular stress also triggers the formation of LLPS to overproduce, sequester, protect or coalesce biological components.[51] Since every living cell performs continuously thousands of different chemical reactions that are mediated by a series of biological catalysts, it is not surprising that LLPS also regulates enzyme activity in biological systems. In this study, we explored a prototypical LLPS system coupled to a glycolytic enzymatic reaction. The enzyme, glucose-6-phosphate dehydrogenase (G6PDH), converts glucose-6-phosphate and the cofactor $NADP^+$ to 6-phospho-D-glucono-1,5-lactone and NADPH, and the droplet phase, which consists of poly-L-lysine (PLL) and NADPH, is dynamically controlled by product formation, i.e., the NADPH concentration. Liquid droplets formed from adenosine triphosphate (ATP) and PLL are well-known *in vitro* model systems and are fairly well characterised.[66–68] Droplets formed by NADPH, on the other hand, have only recently been explored.[53] When NADPH is oxidized to $NADP^+$, no droplets were observed as the positive charge due to oxidation attenuates the interaction with PLL.

We first characterised the temperature and pressure stability of the droplet phase as well as the stability of the enzyme itself under the same conditions, which is a prerequisite for studying the combined effects of temperature, pressure, and the droplet phase on the enzymatic reaction itself. In the low kbar range, pressure-induced dissociation is often observed in oligomeric proteins, whereas the unfolding process of most monomeric proteins tends to occur typically at pressures beyond 4 kbar.[9–11] The enzyme G6PDH exhibits a moderate temperature stability and starts to unfold and aggregate at $T_m \approx 50\,^{\circ}C$, but no significant secondary structural changes were observed in the whole pressure range covered at temperatures below T_m, with minor changes occurring beyond ~3 kbar, only. The liquid-phase droplets generated by NADPH/PLL induced by the G6PDH reaction turned out to be very pressure-stable biomolecular assemblies. Several other liquid condensates (e.g., from γ-crystallin, γ-globulin, ATP/PLL, lysozyme, LAF-1, α-elastin) have been shown to be strongly affected by temperature and pressure to varying degrees.[10,67,69,70] The droplet phase of the two-component NADPH/PLL system is essentially stabilized by electrostatic interactions and most likely very densely packed with few void spaces, rendering the droplet phase pressure stable even up to 2 kbar. The increased thermal motion and the configurational entropy gain at high temperatures leads to disappearance of the droplet phase beyond 60 °C, as expected for such an LLPS system with upper critical solution temperature.

In pure buffer solution, no significant changes in the catalytic efficiency, k_{eff}, were observed with an increase of temperature or pressure, which can be attributed to a compensating effect of K_M and k_{cat}. Conversely, sequestration of the reactants in the liquid droplet phase led to a boost in catalytic efficiency, which was found to be most pronounced at high pressures (Figure 4C). In the crowded environment of the

© 2024 The Authors. Chemistry - A European Journal published by Wiley-VCH GmbH

15213765, 2024, 28, Downloaded from https://chemistry-europe.onlinelibrary.wiley.com/doi/10.1002/chem.202400690 by Technische Universitaet Dortmund, Wiley Online Library on [14/07/2026]. See the Terms and Conditions (https://onlinelibrary.wiley.com/terms-and-conditions) on Wiley Online Library for rules of use; OA articles are governed by the applicable Creative Commons License

droplet phase, a marked increase of the activity of the reactants by mass action (likely also affected by confinement-induced changes in hydration properties) induced a marked increase of the affinity of enzyme and substrate, resulting in a drastic decrease of K_M. In addition, K_M in the droplet phase exhibited only a minor pressure dependence due to a marked decrease of the unfavorable binding volume in the droplet state (Figure 4A, Table 1). The increase in k_{cat} in the droplet phase at high pressure further contributes to the marked increase in k_{eff}. Such an increase in k_{cat} could be due to the stabilization of an active conformation of the enzyme in the condensed droplet phase, i.e., an increase in the population of a particularly productive conformational substate which decreases the free energy of activation. Limitation due to viscosity-increased diffusion rates in the droplet phase does not play a role in this case where the reaction is transition-state limited.

To conclude, enzyme systems coupled with LLPS as shown here may be the key to deciphering sequential biochemical reactions in living cells containing numerous biomolecules. Future studies of such 'active droplets' based on the non-equilibrium dynamics of enzyme-enriched condensates may also exhibit a wealth of novel phenomena including multi-droplet formation, droplet fission and condensate motion.[71] As also shown here, expanding the process parameter space by adjusting temperature and pressure conditions can lead to a further boost in enzymatic activity in the droplet state and may be a means to increase the efficiency of industrial enzyme utilization. After all, these data are also of relevance for deep-sea biologists. A high pressure-stability of the enzyme and a significant increase in catalytic efficiency were observed upon compression of the system up to several hundred bar. Such pressure conditions are encountered by numerous organisms (piezophiles) thriving in the deep sea (with an average pressure of ~ 400 bar), which is probably also the place where life on Earth began.[10,11,72–74] High hydrostatic pressure in concert with liquid droplet formation would not only allow a significant increase in the enzymatic activity of such an enzyme, but the crowded liquid droplet state also leads to a confinement-induced stabilization of the enzymes of extremophilic microbes that thrive under harsh conditions of temperature and pressure.[10,11,72,73]

Acknowledgements

The authors acknowledge funding from the Deutsche Forschungsgemeinschaft (DFG, German Research Foundation) under Germany's Excellence Strategy – EXC 2033 – project number 390677874-RESOLV. R.O. is grateful to the Italian MUR for being granted a research associated position (PON R&I 2014–2020, CUP: E65F21003250003). Open Access funding enabled and organized by Projekt DEAL.

Conflict of Interests

The authors declare no conflict of interest.

Data Availability Statement

The data that support the findings of this study are available from the corresponding author upon reasonable request.

Keywords: Enzymatic reactions · High pressure · LLPS systems · High-pressure stopped-flow kinetics

[1] T. Vulliamy, L. Luzzatto, A. Hirono, E. Beutler, *Blood Cells Mol. Dis.* **1997**, *23*, 302–313.
[2] S. Gómez-Manzo, J. Terrón-Hernández, I. De la Mora-De la Mora, A. González-Valdez, J. Marcial-Quino, I. García-Torres, A. Vanoye-Carlo, G. López-Velázquez, G. Hernández-Alcántara, J. Oria-Hernández, H. Reyes-Vivas, S. Enríquez-Flores, *Int. J. Mol. Sci.* **2014**, *15*, 21179–21201.
[3] P. J. Mason, J. M. Bautista, F. Gilsanz, *Blood Rev.* **2007**, *21*, 267–283.
[4] A. Danişan, D. Ceyhan, I. H. Öğüş, N. Özer, *Protein J.* **2004**, *23*, 317–324.
[5] C. Olive, M. E. Geroch, H. R. Levy, *J. Biol. Chem.* **1971**, *246*, 2047–2057.
[6] L. V. Eggleston, H. A. Krebs, *Biochem. J.* **1974**, *138*, 425–435.
[7] R. Moreno-Sánchez, J. C. Gallardo-Pérez, S. Rodríguez-Enríquez, E. Saavedra, Á. Marín-Hernández, *Free Radical Biol. Med.* **2017**, *112*, 149–161.
[8] G. N. Somero, *Annu. Rev. Physiol.* **1992**, *54*, 557–577.
[9] R. Winter, *Annu. Rev. Biophys. Biomol. Struct.* **2019**, *48*, 441–463.
[10] J.-M. Knop, S. Mukherjee, M. W. Jaworek, S. Kriegler, M. Manisegaran, Z. Fetahaj, L. Ostermeier, R. Oliva, S. Gault, C. S. Cockell, R. Winter, *Chem. Rev.* **2023**, *123*, 73–104.
[11] J. L. Silva, A. C. Oliveira, T. C. R. G. Vieira, G. A. P. de Oliveira, M. C. Suarez, D. Foguel, *Chem. Rev.* **2014**, *114*, 7239–7267.
[12] M. J. Eisenmenger, J. I. Reyes-De-Corcuera, *Enzym. Microb. Technol.* **2009**, *45*, 331–347.
[13] M. W. Jaworek, N. F. Gajardo-Parra, G. Sadowski, R. Winter, C. Held, *Colloids Surf. B.* **2021**, *208*, 112127.
[14] E. Decaneto, S. Suladze, C. Rosin, M. Havenith, W. Lubitz, R. Winter, *Biophys. J.* **2015**, *109*, 2371–2381.
[15] V. V. Mozhaev, R. Lange, E. V. Kudryashova, C. Balny, *Biotechnol. Bioeng.* **1996**, *52*, 320–331.
[16] T. Q. Luong, N. Erwin, M. Neumann, A. Schmidt, C. Loos, V. Schmidt, M. Fändrich, R. Winter, *Angew. Chem. Int. Ed.* **2016**, *55*, 12412–12416.
[17] K. Akasaka, H. Nagahata, A. Maeno, K. Sasaki, *Biophysics (Biophys. Soc. Jpn.)* **2008**, *4*, 29–32.
[18] K. Akasaka, H. Matsuki, *High Pressure Bioscience*, Subcellular Biochemistry Vol. 72, Springer Netherlands, Dordrecht, **2015**.
[19] M. W. Jaworek, V. Schuabb, R. Winter, *Phys. Chem. Chem. Phys.* **2017**, *20*, 1347–1354.
[20] M. L. Toledo, M. M. Pereira, M. G. Freire, J. P. A. Silva, J. A. P. Coutinho, A. P. M. Tavares, *ACS Sustainable Chem. Eng.* **2019**, *7*, 11806–11814.
[21] R. J. Ellis, *Trends Biochem. Sci.* **2001**, *26*, 597–604.
[22] B. Akabayov, S. R. Akabayov, S. J. Lee, G. Wagner, C. C. Richardson, *Nat. Commun.* **2013**, *4*, 1615.
[23] J. A. Dix, A. S. Verkman, *Annu. Rev. Biophys.* **2008**, *37*, 247–263.
[24] I. Pastor, E. Vilaseca, S. Madurga, J. L. Garcés, M. Cascante, F. Mas, *J. Phys. Chem. B* **2010**, *114*, 4028–4034.
[25] B. van den Berg, R. J. Ellis, C. M. Dobson, *EMBO J.* **1999**, *18*, 6927–6933.
[26] J. Ådén, P. Wittung-Stafshede, *Biochemistry* **2014**, *53*, 2271–2277.
[27] J. Li, S. Zhang, C. C. Wang, *J. Biol. Chem.* **2001**, *276*, 34396–34401.
[28] P. H. Schummel, C. Anders, M. Jaworek, R. Winter, *ChemPhysChem* **2019**, *20*, 1098–1109.
[29] L. Stagg, S. Q. Zhang, M. S. Cheung, P. Wittung-Stafshede, *Proc. Natl. Acad. Sci. USA* **2007**, *104*, 18976–18981.
[30] W. M. Aumiller, B. W. Davis, E. Hatzakis, C. D. Keating, *J. Phys. Chem. B* **2014**, *118*, 10624–10632.
[31] C. G. Poggi, K. M. Slade, *Biochemistry* **2015**, *54*, 260–267.
[32] M. G. S. Norris, N. Malys, *Biochem. Biophys. Res. Commun.* **2011**, *405*, 388–392.
[33] C. Balcells, I. Pastor, E. Vilaseca, S. Madurga, M. Cascante, F. Mas, *J. Phys. Chem. B* **2014**, *118*, 4062–4068.
[34] I. Pastor, E. Vilaseca, S. Madurga, J. L. Garcés, M. Cascante, F. Mas, *J. Phys. Chem. B* **2011**, *115*, 1115–1121.
[35] A. Dhar, A. Samiotakis, S. Ebbinghaus, L. Nienhaus, D. Homouz, M. Gruebele, M. S. Cheung, *Proc. Natl. Acad. Sci. USA* **2010**, *107*, 17586–17591.

© 2024 The Authors. Chemistry - A European Journal published by Wiley-VCH GmbH

15213765, 2024, 28, Downloaded from https://chemistry-europe.onlinelibrary.wiley.com/doi/10.1002/chem.202400690 by Technische Universitaet Dortmund, Wiley Online Library on [14/07/2026]. See the Terms and Conditions (https://onlinelibrary.wiley.com/terms-and-conditions) on Wiley Online Library for rules of use; OA articles are governed by the applicable Creative Commons License

[36] K. Totani, Y. Ihara, I. Matsuo, Y. Ito, *J. Am. Chem. Soc.* **2008**, *130*, 2101–2107.
[37] T. Vöpel, G. I. Makhatadze, *PLoS One* **2012**, *7*, 1–6.
[38] L. Homchaudhuri, N. Sarma, R. Swaminathan, *Biopolymers* **2006**, *83*, 477–486.
[39] H.-X. Zhou, G. Rivas, A. P. Minton, *Annu. Rev. Biophys.* **2008**, *37*, 375–397.
[40] A. P. Minton, *J. Biol. Chem.* **2001**, *276*, 10577–10581.
[41] M. Pavlovic, A. Plucinski, J. Zhang, M. Antonietti, L. Zeininger, B. V. K. J. Schmidt, *Langmuir* **2020**, *36*, 1401–1408.
[42] B. Wang, L. Zhang, T. Dai, Z. Qin, H. Lu, L. Zhang, F. Zhou, *Signal Transduction Targeted Ther.* **2021**, *6*, 290.
[43] R. M. Absmeier, G. J. Rottenaicher, H. L. Svilenov, P. Kazman, J. Buchner, *FEBS J.* **2023**, *290*, 1398–1419.
[44] S. Ambadipudi, J. Biernat, D. Riedel, E. Mandelkow, M. Zweckstetter, *Nat. Commun.* **2017**, *8*, 275.
[45] A. Molliex, J. Temirov, J. Lee, M. Coughlin, P. K. Anderson, H. J. Kim, T. Mittag, J. P. Taylor, *Cell* **2015**, *163*, 123–133.
[46] C. P. Brangwynne, P. Tompa, R. V. Pappu, *Nat. Phys.* **2015**, *11*, 899–904.
[47] S. F. Banani, H. O. Lee, A. A. Hyman, M. K. Rosen, *Nat. Rev. Mol. Cell Biol.* **2017**, *18*, 285–298.
[48] Y. Shin, C. P. Brangwynne, *Science* **2017**, *357*, 1253.
[49] B. Saini, T. K. Mukherjee, *J. Phys. Chem. B* **2023**, *127*, 180–193.
[50] C. Love, J. Steinkühler, D. T. Gonzales, N. Yandrapalli, T. Robinson, R. Dimova, T.-Y. D. Tang, *Angew. Chem. Int. Ed.* **2020**, ***59***, 5950–5957.
[51] B. G. O'Flynn, T. Mittag, *Curr. Opin. Cell Biol.* **2021**, *69*, 70–79.
[52] M. Dindo, A. Bevilacqua, P. Laurino, *Seibutsu Butsuri* **2023**, *63*, 12–15.
[53] T. Ura, S. Tomita, K. Shiraki, *Chem. Commun.* **2021**, *57*, 12544–12547.
[54] E. Morild, *Adv. Protein Chem.* **1981**, *34*, 93–166.
[55] L. Ostermeier, M. Ascani, N. Gajardo-Parra, G. Sadowski, C. Held, R. Winter, *Biophys. Chem.* **2023**, *304*, 107128.
[56] M. W. Jaworek, R. Winter, *ChemSystemsChem* **2021**, *3*, e2000029.
[57] P. Bugnon, G. Laurenczy, Y. Ducommun, P. Sauvageat, A. Merbach, R. Ith, R. Tschanz, M. Doludda, R. Bergbauer, E. Grell, *Anal. Chem.* **1996**, *68*, 3045–3049.
[58] P. T. T. Wong, D. W. Armstrong, *Biochim. Biophys. Acta Protein Struct. Mol. Enzymol.* **1992**, *1159*, 237–242.
[59] J. Arrondo, A. Muga, J. Castresana, F. Goñi, *Prog. Biophys. Mol. Biol.* **1993**, *59*, 23–56.
[60] R. Oliva, N. Jahmidi-Azizi, S. Mukherjee, R. Winter, *J. Phys. Chem. B* **2021**, *125*, 539–546.
[61] P. Rowland, A. K. Basak, S. Gover, H. R. Levy, M. J. Adams, *Structure* **1994**, *2*, 1073–1087.
[62] P. Ortiz-Ramírez, B. Hernández-Ochoa, D. Ortega-Cuellar, A. González-Valdez, V. Martínez-Rosas, L. Morales-Luna, R. Arreguin-Espinosa, R. A. Castillo-Rodríguez, L. M. Canseco-ávila, N. Cárdenas-Rodríguez, V. P. de la Cruz, A. M. Montiel-González, F. Gómez-Chávez, S. Gómez-Manzo, *Microorganisms* **2022**, *10*, 1359.
[63] L. Morales-Luna, H. Serrano-Posada, A. González-Valdez, D. Ortega-Cuellar, A. Vanoye-Carlo, B. Hernández-Ochoa, E. Sierra-Palacios, Y. Rufino-González, R. A. Castillo-Rodríguez, V. P. de la Cruz, L. Moreno-Vargas, D. Prada-Gracia, J. Marcial-Quino, S. Gómez-Manzo, *Int. J. Mol. Sci.* **2018**, *19*, 2518.
[64] A. O. Ferrão-Gonzales, S. O. Souto, J. L. Silva, D. Foguel, *Proc. Natl. Acad. Sci. USA* **2000**, *97*, 6445–6450.
[65] P. H. Schummel, M. Gao, R. Winter, *ChemPhysChem* **2016**, *18*, 189–197.
[66] S. Koga, D. S. Williams, A. W. Perriman, S. Mann, *Nat. Chem.* **2011**, *3*, 720–724.
[67] Z. Fetahaj, L. Ostermeier, H. Cinar, R. Oliva, R. Winter, *J. Am. Chem. Soc.* **2021**, *143*, 5247–5259.
[68] T. Lu, K. K. Nakashima, E. Spruijt, *J. Phys. Chem. B* **2021**, *125*, 3080–3091.
[69] Z. Fetahaj, M. W. Jaworek, R. Oliva, R. Winter, *Chem. Eur. J.* **2022**, *28*, e202201658.
[70] H. Cinar, Z. Fetahaj, S. Cinar, R. M. Vernon, H. S. Chan, R. Winter, *Chem. Eur. J.* **2019**, *25*, 13049–13069.
[71] L. Demarchi, A. Goychuk, I. Maryshev, E. Frey, *Phys. Rev. Lett.* **2023**, *130*, 128401.
[72] J. L. Markley, D. B. Northrop, C. A. Royer, *High Pressure Effects in Molecular Biophysics and Enzymology*, Oxford University Press, Oxford, **1996**.
[73] I. Daniel, P. Oger, R. Winter, *Chem. Soc. Rev.* **2006**, *35*, 858–875.
[74] S. Kapoor, M. Berghaus, S. Suladze, D. Prumbaum, S. Grobelny, P. Degen, S. Raunser, R. Winter, *Angew. Chem. Int. Ed.* **2014**, *53*, 8397–8401.

Manuscript received: February 20, 2024
Accepted manuscript online: March 12, 2024
Version of record online: April 10, 2024

© 2024 The Authors. Chemistry - A European Journal published by Wiley-VCH GmbH

15213765, 2024, 28, Downloaded from https://chemistry-europe.onlinelibrary.wiley.com/doi/10.1002/chem.202400690 by Technische Universitaet Dortmund, Wiley Online Library on [14/07/2026]. See the Terms and Conditions (https://onlinelibrary.wiley.com/terms-and-conditions) on Wiley Online Library for rules of use; OA articles are governed by the applicable Creative Commons License